NeuroImage 224 (2021) 117307

Contents lists available at ScienceDirect

NeuroImage

journal homepage: www.elsevier.com/locate/neuroimage

Normative vs. patient-specific brain connectivity in deep brain stimulation

Qiang Wang[a,*], Harith Akram[b,c], Muthuraman Muthuraman[d], Gabriel Gonzalez-Escamilla[d], Sameer A. Sheth[e], Simón Oxenford[a], Fang-Cheng Yeh[f], Sergiu Groppa[d], Nora Vanegas-Arroyave[g], Ludvic Zrinzo[b,c], Ningfei Li[a], Andrea Kühn[a], Andreas Horn[a]

[a] Movement Disorders & Neuromodulation Unit, Department for Neurology, Charité – University Medicine Berlin, Germany
[b] Unit of Functional Neurosurgery, UCL Queen Square Institute of Neurology, Queen Square, London WC1N 3BG, UK
[c] Victor Horsley Department of Neurosurgery, National Hospital for Neurology and Neurosurgery, UCLH, Queen Square, London WC1N 3BG, UK
[d] Movement Disorders and Neurostimulation, Biomedical Statistics and Mulitmodal Signal Processing Unit, Department of Neurology, University Medical Center of the Johannes Gutenberg University, Mainz, Germany
[e] Department of Neurosurgery, Baylor College of Medicine, Houston, TX, USA
[f] Department of Neurological Surgery, University of Pittsburgh Medical Center, Pittsburgh, PA, USA
[g] Department of Neurology, Columbia University College of Physicians and Surgeons, New York, NY, USA

ARTICLE INFO

Keywords:
Deep brain stimulation
Subthalamic nucleus
Parkinson's disease
Human connectome
Tractography

ABSTRACT

Brain connectivity profiles seeding from deep brain stimulation (DBS) electrodes have emerged as informative tools to estimate outcome variability across DBS patients. Given the limitations of acquiring and processing patient-specific diffusion-weighted imaging data, a number of studies have employed normative atlases of the human connectome. To date, it remains unclear whether patient-specific connectivity information would strengthen the accuracy of such analyses. Here, we compared similarities and differences between patient-specific, disease-matched and normative structural connectivity data and their ability to predict clinical improvement.

Data from 33 patients suffering from Parkinson's Disease who underwent surgery at three different centers were retrospectively collected. Stimulation-dependent connectivity profiles seeding from active contacts were estimated using three modalities, namely patient-specific diffusion-MRI data, age- and disease-matched or normative group connectome data (acquired in healthy young subjects). Based on these profiles, models of optimal connectivity were calculated and used to estimate clinical improvement in out of sample data.

All three modalities resulted in highly similar optimal connectivity profiles that could largely reproduce findings from prior research based on this present novel multi-center cohort. In a data-driven approach that estimated optimal whole-brain connectivity profiles, out-of-sample predictions of clinical improvements were calculated. Using either patient-specific connectivity ($R = 0.43$ at $p = 0.001$), an age- and disease-matched group connectome ($R = 0.25$, $p = 0.048$) and a normative connectome based on healthy/young subjects ($R = 0.31$ at $p = 0.028$), significant predictions could be made.

Our results of patient-specific connectivity and normative connectomes lead to similar main conclusions about which brain areas are associated with clinical improvement. Still, although results were not significantly different, they hint at the fact that patient-specific connectivity may bear the potential of explaining slightly more variance than group connectomes. Furthermore, use of normative connectomes involves datasets with high signal-to-noise acquired on specialized MRI hardware, while clinical datasets as the ones used here may not exactly match their quality. Our findings support the role of DBS electrode connectivity profiles as a promising method to investigate DBS effects and to potentially guide DBS programming.

1. Introduction

Deep brain stimulation (DBS) is a well-established treatment for Parkinson's disease (PD), leading to alleviation of motor symptoms and improvement in quality of life (Deuschl et al., 2006; Schuepbach et al., 2013). DBS does not only exert focal effects (i.e. on the subthalamic nucleus; STN) but also affects distributed basal-ganglia-cortico-cerebellar networks (Accolla et al., 2016; Helmich et al., 2012; Horn, 2019; Horn et al., 2017b; Kahan et al., 2019; Lozano and Lipsman, 2013; Muthuraman et al., 2018). While the notion that DBS modulates distributed brain networks is certainly not new, we can now apply advanced MRI methods to study this relationship more deliberately, as has been done in PD (Accolla et al., 2016; Horn, 2019; Kahan et al., 2019;

* Corresponding author.
E-mail address: qiang.wang@charite.de (Q. Wang).

https://doi.org/10.1016/j.neuroimage.2020.117307
Received 22 February 2020; Received in revised form 17 August 2020; Accepted 22 August 2020
Available online 28 August 2020

Treu et al., 2020),Essential Tremor (Al-Fatly et al., 2019), dystonia (Corp et al., 2019) or obsessive-compulsive disorder (Baldermann et al., 2019; Li et al., 2020).

Using preoperative diffusion-weighted imaging (dMRI), Vanegas-Arroyave and colleagues assessed the connectivity patterns of clinically beneficial DBS electrodes in PD patients. Their results suggested that modulation of white matter tracts connecting electrodes to superior frontal gyrus and thalamus were associated with positive clinical improvement (Vanegas-Arroyave et al., 2016). Similarly, Akram and colleagues used preoperatively acquired dMRI to investigate the cortical connectivity patterns associated with treatment efficacy (Akram et al., 2017). Maximal improvement in cardinal motor symptoms was associated with connectivity of DBS electrodes to different cortical regions: tremor control with connectivity to primary motor cortex (M1), bradykinesia with the supplementary motor area (SMA) and rigidity to both prefrontal cortex (PFC) and SMA. These two studies acquired dMRI in each patient preoperatively. While this approach represents the gold-standard of practice, and variability in fibertracts has been shown in the DBS context (Makris et al., 2016), a practical limitation is that resulting cohort sizes will often be small, studies costly and pooling across centers non-straightforward due to data-heterogeneity. Furthermore, preoperative dMRI data is not routinely acquired preoperatively in a large fraction of DBS patients and cannot be acquired postoperatively (without substantial constraints). This is especially relevant in novel indications such as Alzheimer's Disease (Baldermann et al., 2018; Ponce et al., 2016) or psychiatric indications (Hamani et al., 2011; Huys et al., 2019) where limited numbers of patients undergo surgery, even on a worldwide scale. The same applies to "classical diseases" (such as dystonia) that are treated with unconventional targets (such as the STN), again resulting in a low number of available patients, world-wide (Ostrem et al., 2011; Yao et al., 2019).

A potential approach to overcome this limitation is to substitute individualized dMRI data with normative connectomes – i.e. atlases of average brain connectivity calculated from large cohorts of subjects (Ewert et al., 2018; Horn et al., 2014a, 2019; Horn and Blankenburg, 2016; Marek et al., 2011; Thomas Yeo et al., 2011; Yeh et al., 2018; Yeh and Tseng, 2011). A first study that explored this concept investigated functional and structural connectivity profiles of the ventral intermediate nucleus of the thalamus (Horn et al., 2017a). A second study then investigated optimal connectivity profiles for STN-DBS (Horn et al., 2017b). In this study, the optimal connectivity profiles were estimated on one cohort from a first DBS center and used to predict the motor outcome in patients operated at a different DBS center (Horn et al., 2017b). Specifically, structural and functional connectivity between DBS electrodes and other brain regions were correlated with UPDRS-III changes across patients. This resulted in an optimal connectivity 'fingerprint' of effective DBS electrodes. To validate these maps of optimal connectivity, similarity indices between each electrode's connectivity profile from an independent cohort and the 'optimal' fingerprint were calculated. These were then correlated with empirical clinical improvement.

The concept has since been applied to explore connectivity associated with clinical or behavioral changes in multiple diseases (Al-Fatly et al., 2019; ;Johnson, et al., 2020 Baldermann et al., 2019; de Almeida Marcelino et al., 2019; Li et al., 2020; Neumann et al., 2018; Irmen et al., 2020; Treu et al., 2020). With the increasing popularity of this approach, it is timely to compare results achieved by examining patient-specific connectivity with those obtained using normative connectivity data. One main limitation of the normative connectome approach is that connectivity data taken from atlases will never represent individual differences in connectivity profiles from the actual DBS patients of study. Thus, the use of connectome atlases has clear similarities to the use of other atlases. For instance, histological atlas information was applied to inform DBS for decades (Schaltenbrand G, 1977; Talairach and Tournoux, 1988). Similarly, subcortical atlases – for instance of the STN – have been widely applied to study DBS electrode placement (for an overview see Ewert et al., 2018). However, despite conceptual similarities to other atlases, some aspects of connectome atlases are novel and require further study.

Here, we have retrospectively analyzed individual connectivity estimates that were based on diffusion imaging data (dMRI) scanned from each individual patient before undergoing STN-DBS surgery. In a second step, we substituted these data with either a disease- and age-matched group connectome acquired in different PD patients or a normative connectome acquired in young/healthy subjects. It should be emphasized that the latter was of superior quality and acquired on specialized MRI hardware (Setsompop et al., 2013) while the age-/disease-matched connectome was of largely comparable quality as patient-specific data. The analysis reproduced workflows that were previously published using normative datasets. finally, we compared the amount of variance in clinical improvements that could be estimated using individualized dMRI data versus either of the two group connectome atlases. By doing so, we explored the specific similarities and differences between these types of connectivity information when seeding from DBS electrodes to the rest of the brain.

2. Materials and methods

2.1. Patient cohorts and imaging

Thirty-three DBS patients from 3 different DBS centers (Center 1 (London): $N = 17$, Center 2 (Mainz): $N = 12$, Center 3 (New York): $N = 4$) were included in this retrospective study. Patient demographics are summarized in Table 1.

All patients underwent stereotactic DBS surgery for treatment of PD and received bilateral DBS electrodes (Table 1). Patients had been enrolled following the standard procedure to screen for eligibility of DBS which excluded structural brain abnormalities or severe psychiatric contraindications. Surgical planning was performed based on MRI imaging and DBS lead localizations were verified by microelectrode recording during surgery and intraoperative macrostimulation for the New York and Mainz centers. Specifically, STN-cells were observed by a team of neurologists while slowly advancing the microelectrodes from 10 mm distance toward the target. Cell activity were manually classified into either no cell activity, cell activity of unknown origin or cell activity clearly attributable to either STN or SNr by one or two expert raters. This information was used to verify the lead or to move to a different trajectory. Postoperative imaging was carried out to verify accurate electrode placement in all cohorts (see below). Specifically, the postoperative imaging parameters were as follow. Center 1: postoperative MRI 0.39 × 0.39 × 2.00 mm; Center 2: postoperative MRI 0.83 × 0.83 × 0.80 mm; Center 3: patient #1 postoperative MRI 0.51 × 0.51 × 1.40 mm, patient #2 postoperative CT 0.47 × 0.47 × 1.25 mm, patient #3 postoperative CT 0.46 × 0.46 × 1.0 mm, patient #4 postoperative CT 0.55 × 0.55 × 1.25 mm. Clinical variables including age, sex, disease duration before surgery, L-DOPA equivalent dose (LEDD) at baseline were recorded. Clinical improvement was measured by comparing Unified Parkinson's Disease Rating Scale Part III (UPDRS-III) scores OFF medication preoperatively (baseline) and postoperatively ON DBS OFF medication. Improvement was expressed as percentage improvement between the two scores. This study was approved by the local ethics committee of the Charité, University Medicine Berlin (master vote EA2/186/18). The study in London received ethical approval from the West London NHS Research Ethics Committee (10/H0706/68). At Columbia and Mainz University, all procedures were also approved by the local Institutional Review Board.

2.2. Preoperative diffusion MRI acquisition

Center 1: For details on the London dataset, please see (Akram et al., 2017). Briefly, imaging data were acquired on a 3T Siemens Magnetom Trio TIM Syngo MR B17 using a padded 32-channel receive head

Table 1
Patient demographics of cohorts analyzed.

Cohort	No. (female)	Age, [years]	Disease Duration, [years]	UPDRS-III baseline, OFF medication	LEDD Reduction [%]	Clinical Assessment	UPDRS-III postop, OFF medication	Preop Imaging	dMRI resolution	Postop Imaging	Registration Modalities	Electrode type
Center 1	17(4)	59.9±2.3	11±1.1	50.5±4.3	60±4.1	On vs OFF one year postop	27±3	T1, T2, PD*, R1, R2*, MT	1.5 × 1.5 × 1.5	MRI	T1, T2, PD*, R1, R2*, MT,	3389 Medtronic
Center 2	12(3)	66.7±2.4	15.7±1.1	34.1±2.2	64.7±6.2	On vs OFF 6 months postop	14.9±1.8	T1, T2	2 × 2 × 2	MRI	T1, T2,	3389 Medtronic
Center 3	4(0)	59±3.7	12.3±1.3	31±1.9	58±18.2	On vs OFF 2.5-7 months postop	13.8±3.2	T1, T2	1.88 × 1.88 × 2.6T	MRI,	T1, T2,	3387, 6179, BostonSci Vercise 8 contact linear

PD*, effective proton density; R1, 1 mm high-resolution maps of the longitudinal relaxation rate (R1 = 1/T1)); R2*, effective transverse relaxation rate (R2* = 1/T2*)); MT, magnetization transfer saturation.

coil to reduce discomfort and head motion. Siemens' 511E-Advanced Echo Planar Imaging Diffusion WIP was used. In-plane acceleration was used (GRAPPA factor of 2) with partial Fourier 6/8. In-plane resolution was 1.5 × 1.5 mm^2 (Field of view 219 × 219 mm^2, TR = 12,200 ms, TE = 99.6 ms) and 85 slices were acquired with a 1.5 mm thickness. Diffusion-weighting with b = 1500 s/mm^2 was applied along 128-directions uniformly distributed on the sphere and seven b = 0 s/mm^2 volumes were acquired. To correct for distortions all acquisitions were repeated with reversed phase encoding direction (left to right and right to left phase encode) giving a total of 270 volumes acquired ([128 + 7] × 2). The total acquisition time for the dMRI sequences was 62 min.

Center 2: Diffusion-weighted imaging from Mainz were acquired with 32-directions at b = 1000 s/mm^2 and one b = 0 s volume images for each acquisition (TR=11855 ms, TE=59 ms, fat saturation "on", 60 contiguous slices). dMRI of the whole brain at 2 mm isometric voxel resolution covering a field of view of 224 × 224 mm was obtained. The total acquisition time for the whole protocol was 35 min which included 24 min (3 × 8 min) for dMRI sequences.

Center 3: The diffusion weighted image sequences from New York cohort were acquired with 64-directions at b=1000 s/mm^2 and 6 b = 0 s/mm^2 volumes were also acquired. In-plane resolution was 1.88 × 1.88 mm^2 (TR=8500 ms, TE=108 ms, slice thickness=2.50 mm). To correct for distortions, three acquisitions (2 b = 0 s/mm^2 and 1 b = 1000 s/mm^2 volumes) were repeated with a reversed phase encoding direction (left to right and right to left phase encode) giving a total of 73 components ([64 + 6] + 3). The total acquisition time for the dMRI sequences was 10 min.

2.3. Diffusion pre-processing and tractography

For all but the Mainz cohort (where only one b0 volume was acquired), the diffusion data were acquired with reversed phase-encode blips (left-to-right and right-to-left), resulting in pairs of images with distortion going in opposite directions. From these pairs, the susceptibility induced off-resonance field was estimated using a method described by Andersson et al. (2003) as implemented in FSL (Smith et al., 2004) and the two images were combined into a single corrected one using Topup as implemented in FSL v5.0. The output from Topup was then fed into Eddy (FSL v5.0) for correction of eddy current distortions and subject movement (Andersson and Sotiropoulos, 2016). In the Mainz cohort, only Eddy was applied.

Tractography was performed using the generalized Q-sampling imaging method (Yeh et al., 2010) as implemented in DSI studio (http://dsi-studio.labsolver.org) using the default parameter sets implemented in Lead-Connectome (www.lead-connectome.org; Horn et al., 2014b), which performed whole-brain fiber tracking in patient space and transformed of the tractogram into ICBM 2009b Nonlinear Asymmetric ('MNI') space (Fonov et al., 2011). Whole-brain tractograms were estimated by random-sampling of seedpoints within a white-matter mask defined by (i) segmenting structural (T1 and T2) imaging data using the New Segment approach as implemented in SPM12 (Ashburner and Friston, 2005) and (ii) linearly co-registering the mask to b0-space. In total, 200,000 fiber streamlines were estimated in each patient. Tractograms were then nonlinearly warped into standard space using Advanced Normalization Tools (ANTs; stnava.github.io/ANTs/; Avants et al., 2008) and the "Effective: Low Variance + subcortical refinement" preset implemented in Lead Connectome (Ewert et al., 2019a). Naturally, the same warp was used as in the process of transferring DBS electrodes into standard space (see below). To investigate the role of diffusion-artifacts (especially in the cohort from center 3, where diffusion-correction was not available), we repeated the analysis but instead nonlinearly co-registered between diffusion and anatomical space using a linear stage followed by a SyN stage with default parameters.

2.4. Localization of DBS electrodes and VTA estimation

DBS electrodes were localized using Lead-DBS (https://www.lead-dbs.org/; Horn and Kühn, 2015) in its current (version 2.2.3; Horn et al., 2019) using PaCER (Husch et al., 2018) or the TRAC/CORE approach (Horn and Kühn, 2015) for either postoperative CT or MRI, respectively. Briefly, postoperative CT or MRI were linearly co-registered to preoperative MRI using ANTs. Subcortical refinement was applied as implemented in Lead-DBS to correct for brain shift that may have occurred during surgery. All preoperative volumes were then normalized into MNI space applying the same deformation fields calculated in previous steps mentioned above.

Based on the long-term DBS settings, volumes of tissue activated (VTA) were estimated using a Finite Element Method (FEM)-based model as implemented in Lead-DBS (Horn et al., 2019). This model estimates the E-field (i.e. the gradient distribution of the electrical charge in space measured in Volts per millimeter) on a tetrahedral four-compartment mesh that accounts for grey and white matter, electrode contacts and insulating parts. Grey matter was defined by components of the DISTAL atlas (Ewert et al., 2018) (STN, internal and external pallidum, red nucleus). The electric field (E-field) distribution was then simulated using an adaptation of the FieldTrip-SimBio pipeline (Vorwerk et al., 2018) that has been integrated into Lead-DBS (https://www.mrt.uni-jena.de/simbio/; http://www.fieldtriptoolbox.org/). The E-Field gradient was thresholded for magnitudes above a commonly used value of 0.2 V/mm to define the extent and shape of the VTA (Astrom et al., 2015). VTAs were warped into template space (2009b NLIN ASYM "MNI" Space, Fonov et al., 2011) by applying the same warp of the ANTs registration to VTA files. This is the space in which both group connectomes were available and hence, VTAs were used as seeds in this space. Fig. 1 provides an overview of the methodology applied.

2.5. Structural connectivity estimation

Whole-brain structural connectivity profiles seeding from bilateral VTA in each patient were calculated using three different approaches: First, patient-specific dMRI data were processed for each patient, individually. Second, a disease- and age-matched connectome was estimated based on a cohort of 85 Parkinson's Disease patients acquired within the Parkinson's Progression Markers Initiative (PPMI). Third, connectivity profiles were estimated based on a state-of-the-art multi-shell dMRI dataset based on 32 healthy young subjects that were scanned on specialized MRI hardware within the Human Connectome Project (HCP). The latter two group connectomes were created by performing whole-brain tractography in each individual patient/subject, normalization of tracts (using the same methods as in the present study) and aggregation of tracts across patients/subjects. This led to whole-brain tract-density images seeding from VTAs for each patient based on patient-specific, age-/disease-matched and healthy-/young connectivity data.

Patient-specific dMRI data: Each patient's specific connectome was based on dMRI data acquired pre-operatively. Using the generalized q-sampling imaging approach (which was applied in all three modalities) as implemented in DSI Studio (http://dsi-studio.labsolver.org/, Yeh et al., 2010), a whole-brain set of 200,000 fiber tracts was estimated using the default processing stream of Lead Connectome. This led to one set of (whole-brain) tract-density volumes for each patient.

Age-/disease-matched connectome: dMRI data from 85 patients were obtained from the Parkinson's Progression Markers Initiative (PPMI) database (Marek et al., 2011) and processed using DSI Studio/Lead-Connectome in the same fashion as described above. This PPMI connectome of PD patients that is approximately age- and sex-matched to our full cohort was previously computed (Ewert et al., 2018) and has been used in DBS studies, before (Horn et al., 2017b; Irmen et al., 2019; Neumann et al., 2018). The underlying dMRI data had been acquired in 64 gradient-directions at $b = 1000$ s/mm^2. In-plane resolution was 1.98 × 1.98 mm and 72 slices with a 2 mm thickness were acquired. Detailed scanning parameters can be found on the project website (www.ppmi-info.org), processing details are reported in Ewert et al. (2018).

Young/healthy connectome: dMRI data from 32 healthy young subjects of the Human Connectome Project at Massachusetts General Hospital (https://ida.loni.usc.edu/login.jsp, Setsompop et al., 2013) were obtained and processed using DSI Studio/Lead-Connectome in the same fashion as described above. This 'MGH Adult Diffusion' dataset of the HCP was acquired using state-of-the-art scanning sequences on specialized hardware and from a quality perspective may be considered as one of the best openly available, in-vivo dMRI datasets. Diffusion-weighting with $b = 1000$ s/mm^2 and 3000 s/mm^2 was applied along 64 directions. Furthermore, additional shells at b-values of 5000 and 10,000 s/mm^2 were applied along 128-directions. In-plane resolution was 1.5 × 1.5 mm and 96 slices with a 1.5 mm thickness were acquired.

Structural connectivity between each VTA and voxels in the rest of the brain was estimated using the above connectome datasets and led to whole-brain fiber-density maps as produced by the Lead Connectome Mapper software (Horn et al., 2019). To do so, fibers traversing through VTA were selected from the group connectome and projected to volumetric space of the brain in template space of 2 mm isotropic resolution, denoting the number of fibers (connected to the VTA) that traversed through each voxel. To ensure this didn't affect results, the step was repeated by exporting density-maps in 1 mm resolution. In addition, to explore the similarity and differences between patient-specific and young-/healthy, age-/disease-matched connectivity in specific cortical regions we added a region-of-interest (ROI) analysis. Here, structural connectivity to primary motor cortex (M1), supplementary motor area (SMA), pre-supplementary motor area (pre-SMA) and dorsomedial PFC as defined by the HMAT (Mayka et al., 2006) and Brainnetome atlases (Fan et al., 2016) were calculated. ROIs were chosen from prior literature-informed hypotheses (Akram et al., 2017; Vanegas-Arroyave et al., 2016), indicating that effective DBS was associated with connectivity to these brain structures.

2.6. Estimating a model of optimal connectivity profiles

To estimate a model of optimal connectivity, structural connectivity (tract-density) maps (based on either patient-specific, age- and disease-matched or young/healthy data), seeding from bilateral VTA were Spearman rank-correlated with %-UPDRS-III change across patients in a voxel-wise fashion. This led to a map that showed positive or negative associations with UPDRS-III improvements (henceforth referred to as *R-maps*). Spearman's correlation was used because structural connectivity results are generally non-Gaussian distributed (Horn et al., 2014b). R-maps denote to which areas connectivity is associated with beneficial or detrimental outcomes. By doing so, their spatial distribution is a direct estimate of the optimal connectivity profile of STN-DBS electrodes for PD. In case of patient-specific connectivity, for methodological considerations, two pathways were chosen to derive at group-level R-maps. The first (which is equivalent to the pathway used in case of normative connectomes) involved warping fibertracts to template space and aggregating tract-density maps there (from which R-maps were calculated). The second created tract-density maps in native space (from unnormalized fibertracts) and ported these maps into template space to create R-maps. This was done to rule out effects introduced by the order of processing steps.

2.7. Estimating improvement in out-of-sample patients

To estimate DBS outcome in out-of-sample data, spatial correlations between the optimal structural connectivity model (defined by data-driven R-maps or a previously published optimal model from 2017b) and the VTA-derived structural connectivity profile in each patient were

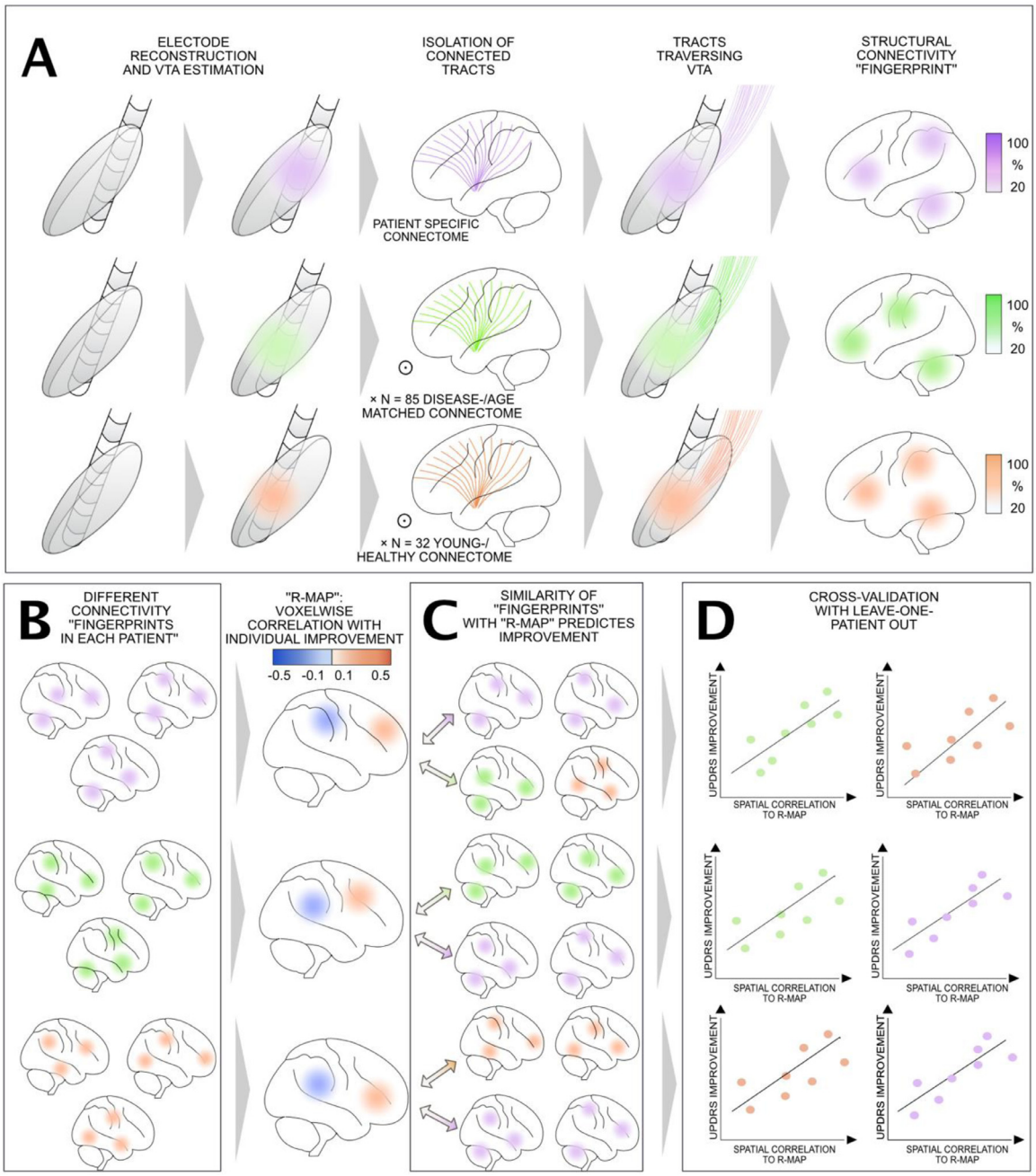

Fig. 1. Applied methodological pipeline of data analysis: (A) For each patient, DBS leads were localized in MNI space using Lead-DBS software, and volumes of tissue activated (VTA) were estimated based on the actual DBS stimulation parameters. Streamlines representing traversing through each patient's VTA to the rest of the brain were selected from either patient-specific dMRI data, an age- and disease-matched group connectome or a young-/health group connectome, resulting in DBS stimulation-dependent connectivity "fingerprints". (B) Connectivity "fingerprints" were obtained for each patient using each of the three sources of connectivity data. Across each group of patients, an optimal connectivity profile (R-Map) was generated by correlating connectivity fingerprints with UPDRS-III improvement. (C) R-maps represent models for "optimal" connectivity fingerprints. Comparing similarities between each new (out-of-sample) patient's connectivity fingerprint with these models (by means of spatial correlation), clinical improvements can be estimated (shown in D for a leave-one-out design).

calculated. For instance, in some analyses, this was done in a leave-one-out fashion (i.e. data from patients #1-32 were used to create an R-map, which was then compared to the connectivity map of patient #33 to estimate improvement in this patient. The same was iteratively done for all patients.). The resulting similarity indices – again expressed as a (spatial) Spearman's rank correlation coefficients – estimate 'how optimal' each connectivity profile was and used to explain the variance in clinical improvement (%-UPDRS-III improvement) in a linear regression model.

Throughout the paper, we used randomized permutation tests (5000 permutations) to test for significance (at a 0.05 significance level) and all analyses were carried out in MATLAB (The Mathworks, Natick, MA).

3. Results

Our DBS cohort included 33 patients enrolled at 3 independent centers (7 females, mean age 62.5 ±1.6 years). The average disease duration in the entire sample was 12.9 ±0.8 years. Reduction in LEDD comparing baseline to post-DBS on average was 61.5 ±3.6%. Baseline UPDRS-III score was 42.0 ±2.8, postoperative score 28.1 ±2.1 points (leading to a 51.0 ±3.0% improvement). LEDD reduction and UPDRS-III

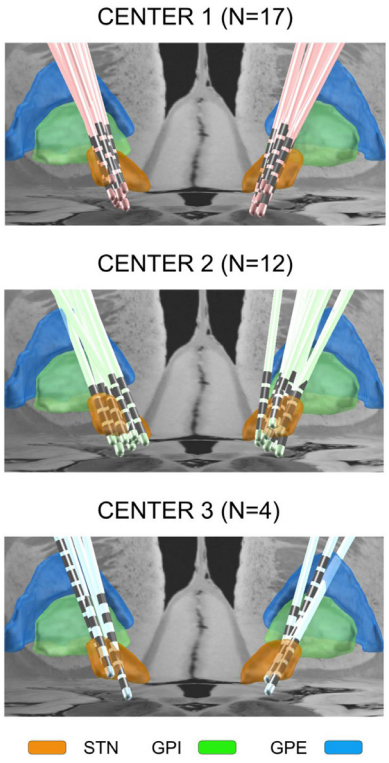

Fig. 2. DBS electrode reconstructions in the three cohorts from the three centers. Subcortical structures are defined by the DISTAL Atlas (Ewert et al., 2018), axial and coronal planes of the 7T MRI *ex vivo* human brain template shown (Edlow et al., 2019).

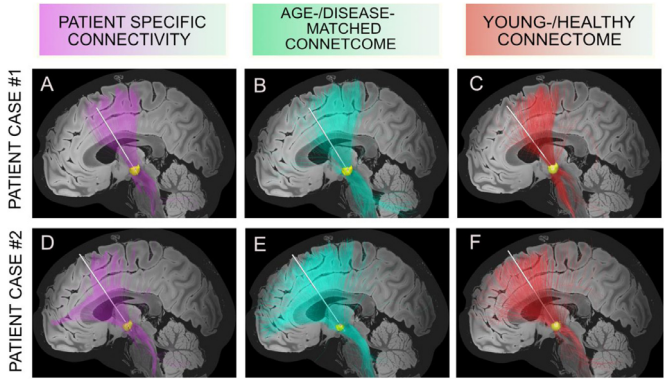

Fig. 3. Two representative examples of structural connectivity between individual DBS sites (left hemisphere) and the rest of the brain based on patient-specific connectivity, the disease- and age-matched connectome and young-/healthy connectome. A sagittal plane of the 7T MRI *ex vivo* human brain template (Edlow et al., 2019) is shown at $x = 3$ mm. The yellow sphere represents the VTA. While in most patients, connectivity profiles were largely similar using either method (as in case #1), few patients had differing results across methods (as in case #2).

improvements were not significantly different across the three datasets ($p > 0.05$ for both variables). Of all patients, 4 were tremor-dominant, 21 were akinetic rigid and 8 were mixed following criteria defined in Eggers et al. (2011).

DBS electrode placement was comparable across the three cohorts (Fig. 2, see also Fig. S1) and structural connectivity profiles from two typical patient cases are shown in Fig. 3. Distances between active electrode centers and the closest voxel center in the STN were calculated and this was used to estimate how many electrode contacts were inside (< 1 mm), at the border (1–2 mm) or outside (>2 mm) of the STN (given a diameter of the electrodes of ~1.24 mm and a voxel-size of 0.22 mm in the STN atlas). 57 contacts were inside, 8 at the border region and 4 outside the STN (also see Figs. S2 and S3).

Table 2
Correlations between connectivity metrics. *R*-values show agreement between connectivity estimates connecting VTAs to M1, SMA, pre-SMA, and PFC across the group of patients. For instance, the first entry denotes that connectivity strength between VTAs and M1 estimated using patient-specific connectivity (i) and an age-/disease-matched connectome (ii) correlated by a Spearman's rho of 0.73. Note that similarities between patient-specific and group-level data become lower when advancing in frontal direction while it remains high between normative connectomes. (iii) stands for the young-/healthy connectome.

	M1	SMA	pre-SMA	PFC
i vs ii	*R*=0.73, *p*=0.004	*R*=0.43, *p*=0.009	*R*=0.33, *p*=0.062	*R*=0.18, *p*=0.17
i vs iii	*R*=0.57, p=0.004	*R*=0.40, *p*=0.015	*R*=0.33, *p*=0.044	*R*=0.21, *p*=0.17
ii vs iii	*R*=0.85, *p*=0.001	*R*=0.85, *p*=0.001	*R*=0.70, *p*=0.002	*R*=0.96, *p*=0.001

(i) patient-specific connectivity, (ii) age-/disease-matched connectivity and (iii) young-/health connectivity.

Average volumes of VTAs were 149 ±68 mm^3 (left) and 175 ±118 mm^3 (right). This led to connections of 2999 ±1363 of streamlines per VTA in patient-specific data, 27,548 ±8951 in the age-/disease-matched connectome data and 21,875 ±17,791 in the healthy/young connectome. On average, spatial correlations amounted to $R = 0.39$ ±0.05 between patient-specific and age-/disease-matched connectivity (across the whole brain), to $R = 0.38$ ±0.05 between patient-specific data and the young/healthy connectome and to $R = 0.58$ ±0.05 between the healthy/young and age-/disease-matched connectomes. This was the case for most patients, and fibers predominantly connected to the sensorimotor strip (M1, SMA or pre-SMA). Only in a few patients did patient-individual structural connectivity estimates differ largely (for an example see bottom row of Fig. 3).

Correlations between patient-specific and young-/healthy connectivity estimates across the group of patients were high for apical cortical regions but lower for more frontal regions (see Fig. S5). Specifically, connectivity estimates between electrodes and these regions as estimated from patient-specific versus the healthy-/young connectome correlated across patients: primary motor cortex: $R = 0.57$, $p = 0.004$, supplementary motor area: $R = 0.40$, $p = 0.015$, pre-supplementary motor area pre-SMA: $R = 0.33$, $p = 0.044$ and dorsomedial prefrontal cortex: $R = 0.21$, $p = 0.17$. Furthermore, an outliner analysis using skipped correlations as implemented in the robust correlation toolbox (Pernet et al., 2013) was performed to further confirm these results (Table S1). Furhter correlations between patient-specific and age-/disease- matched connectivity, young-/healthy and age-/disease-matched connectivity are shown in Table 2. *P*-values were corrected for multiple comparisons using the Bonferroni–Holm method.

In Horn et al., 2017b, an R-map that defined optimal connectivity values was estimated based on a two-center cohort of $N = 95$ patients. Here, this R-map was used to account for a certain percentage of outcome in the presnet independent three-center cohort based on individualized diffusion data (Fig. 4; $R = 0.28$, $p = 0.045$). When instead using the age- and disease-matched connectome ($R = 0.30$, $p = 0.031$) or the young-/healthy connectome ($R = 0.33$, $p = 0.021$), correlations remained significant. These estimates were not significantly different from each other in head-to-head comparisons based on a Fisher r-to-z transformation ($p > 0.8$ for all comparisons).

In a next step, we calculated data-driven optimal connectivity maps (R-maps) from scratch based on the presnt three-center cohort using patient-specific dMRI, the age-/disease-matched connectome or the young-/healthy connectome, respectively. Using either metric, connectivity to primary motor cortex (M1) and primary somatosensory cortex

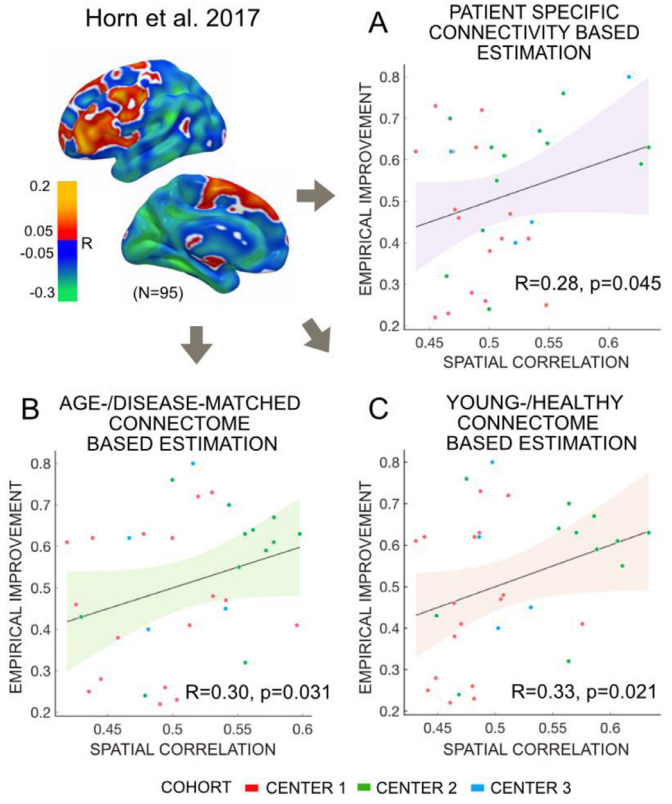

Fig. 4. Validation of optimal connectivity profiles estimated in, Horn et al., 2017b) on the present three-center cohort (N = 33), in which individual dMRI data was available. Clinical improvements could be significantly estimated using patient-specific connectivity (A), a disease-/age-matched connectome (B) and a young-/healthy connectome (C).

(S1) was negatively correlated with DBS outcome. In contrast, connectivity to pre-SMA, anterior cingulate and medial frontal cortices was associated with beneficial DBS outcome (Fig. 5).

All three metrics, i.e. patient-specific connectivity (R = 0.43; p = 0.001), age-/disease-matched connectome (R = 0.25; p = 0.048) and healthy-/young connectome (R = 0.31; p = 0.028) could account for a significant part of the variance in clinical outcome in a leave-one-out design (Fig. 5). In case of patient-specific connectivity, a second analysis pathway (see methods) was tested, that led to inferior results (R = 0.35, p = 0.017, see Fig. S6). Based on these values, we conclude that ~6–18% of the variance in clinical outcomes could be explained in out-of-sample data. Furthermore, to investigate effects of distortion artifacts in diffusion imaging, the analysis (following the first pathway) was repeated but applying a non-linear registration strategy between diffusion and anatomical space. This reduced correlations from R = 0.43 to R = 0.37 at p = 0.011. Finally, to rule out effects introduced by downsampling of spatial similarity steps, the main analysis was repeated after exporting tract-density maps in 1 mm resolution (as opposed to 2 mm as above). Results remained highly similar (R = 0.42 at p = 0.002 for patient-specific connectivity; R = 0.27, p = 0.041 for the age- and disease-matched group connectome; R = 0.31 at p = 0.032 for the healthy-/young connectome).

Frame-to-frame displacements within individual dMRI volumes were 0.31 ±1.64 mm on average, rotation 0.003° ±0.001°, respectively. Specific head motion information (rotation/translation) of individual patients is reported in Table S2. Head motion, including the displacement and rotation across each dataset did not explain prediction errors in our main analysis (R^2 = 0.03 at p = 0.63). To further assess whether head motion played a significant role, we repeated the aforementioned analysis using patient-specific connectivity data after excluding dMRI volumes that were affected by the top 2% of head motion/rotation. Connectomes were then calculated again, and the analysis was repeated. Results remained identical (R = 0.41 at p = 0.009; Fig. S7).

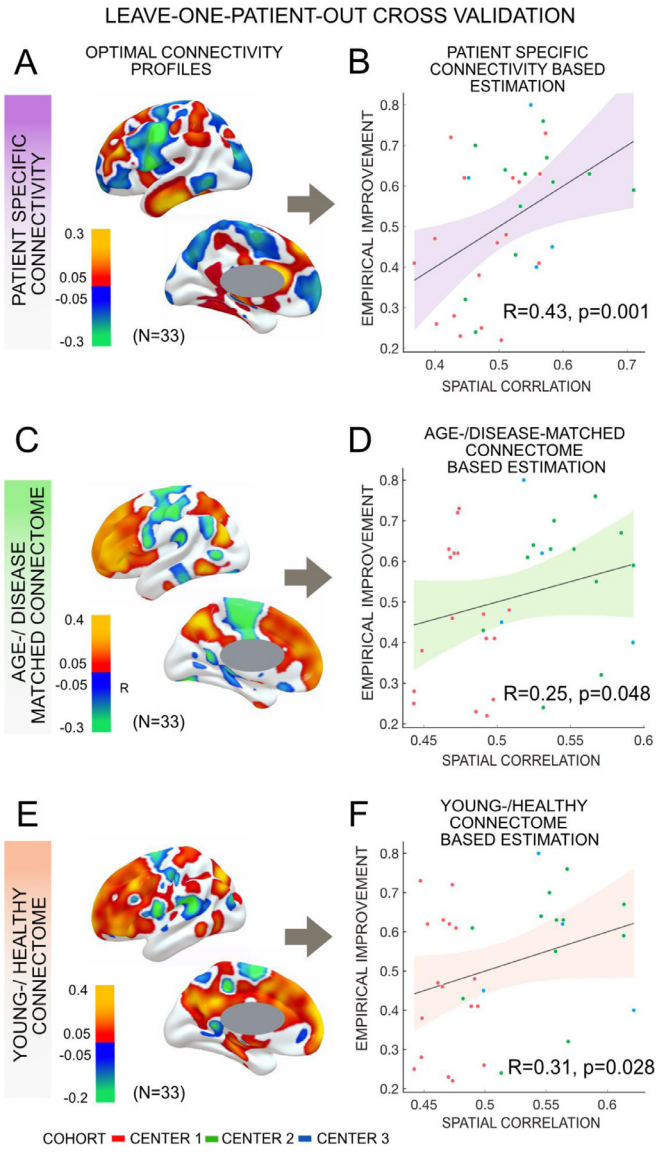

Fig. 5. Structural connectivity (patient-specific connectome, age-/disease-matched and healthy-/young) estimated change in UPDRS-III score using a leave-one-patient-out model (N = 33). Optimal structural connectivity model generated with patient-specific connectome (A), age-/disease-matched connectome (C) and young-/healthy connectome (E) effectively estimated patient's improvement based on respective connectome (B, D, F). Slightly more variance was estimated from the patient-specific connectivity model than the other two metrics. Please note that values shown on the R-maps are not necessarily significant since mass-univariate tests were applied. Rather, the spatial profile of these maps was used to make predictions in out-of-sample data which are then tested for significance.

Finally, this main analysis was repeated when thresholding R-maps to account for positive values, only. Again, this led to similar correlations while amounts predicted by the patient-specific analysis decreased most (R = 0.35 at p = 0.012 for patient-specific connectivity, R = 0.27, p = 0.046 for the age- and disease-matched group connectome and R = 0.43 at p = 0.002 for healthy-/young connectome).

Correlations derived from either metric were not significantly different from each other in head-to-head comparisons based on a Fisher r-to-z transformation (p > 0.4 for all comparisons). Furthermore, cross-estimates between metrics were poorer and not significant, i.e. when the R-map was based on a group connectome, but structural connectiv-

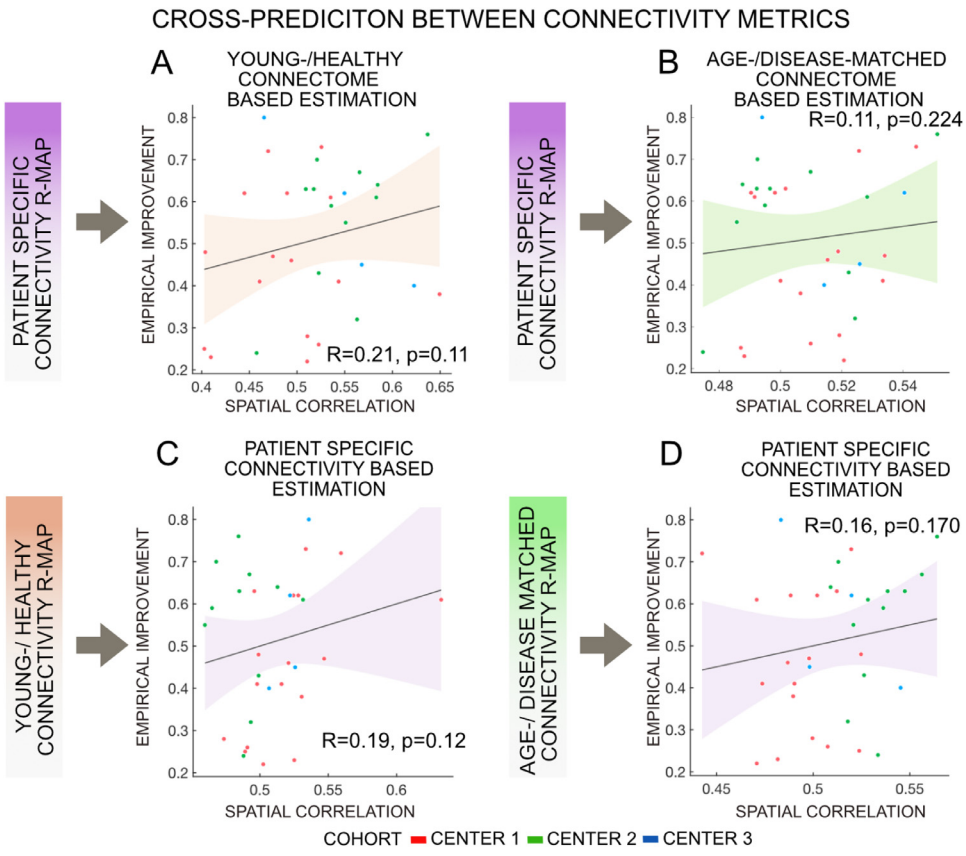

Fig. 6. Structural connectivity (patient-specific, age-/disease-matched, healthy-/young connectome) cross-prediction change in UPDRS-III scores under STN-DBS. Patient-specific connectivity couldn't explain patient's change following DBS based on healthy-/young connectome (A) and age-/disease-matched connectome (B). Similarly, R-Map generated with young-/healthy connectome (C) and age-/disease-matched connectome (D) could not estimate patient's improvement based on patient-specific connectome.

ity maps were based on patient-specific structural connectivity or vice versa (Fig. 6). This is not-surprising since normative and patient-specific connectivity estimates are not completely interchangeable. Still, it may underline the importance of consistency in the choice of metric when performing such dMRI based connectivity analyses.

4. Discussion

Three main conclusions may be drawn from the present study. First, findings confirm a previously published model of optimal STN-DBS electrode connectivity based on a novel independent sample of patients operated in three different centers (Horn et al., 2017b). Crucially, while the original model had been derived from normative connectivity estimates, patient-specific dMRI data was successfully used to account for DBS outcome in the present cohort. Second, we show that optimal connectivity maps defined using individualized data are highly similar to the ones defined using group connectomes. Irrespective of using patient-specific, age-/disease-matched or healthy-/young connectome data, structural connectivity to pre-SMA, anterior cingulate and medial frontal cortices was associated with beneficial DBS outcome. However, third, the amount of variance in clinical improvement explained by either method was not exactly the same. While none of the metrics resulted in significantly higher predictions than the other two, the use of patient-specific connectome data resulted in the highest *R*-value between estimated and empirical improvements ($R = 0.43$ vs. 0.31 or 0.25). This was true although the quality of the patient specific diffusion datasets differed between the three centers resulting in an 'overall' poorer data quality than found in normative connectomes.

4.1. Normative group connectomes vs. patient-specific connectivity

Recently, normative structural connectomes were introduced to account for motor improvements (Horn et al., 2017b; Treu et al., 2020) and changes in depressive symptoms (Irmen et al., 2020) in Parkinson's disease patients following STN-DBS. The concept was also applied to DBS in Essential Tremor syndrome (Al-Fatly et al., 2019), Obsessive-Compulsive disorder (Baldermann et al., 2019; Li et al., 2020) and Epilepsy (Middlebrooks et al., 2018). Furthermore, normative connectomes were used to explain behavioral effects following STN-DBS such as movement speed (Neumann et al., 2018) and motor learning (de Almeida Marcelino et al., 2019) or stopping of ongoing movements (Lofredi et al. 2020). Finally, the concept was applied to investigate side-effects such as DBS induced seizures (Boutet et al., 2019), weight-changes (Baldermann et al., 2019) or panic attacks (Elias et al., 2019). While the approach was sucessful to explain variance in clinical improvement in out-of-sample data (i.e. models were learned on one cohort to predict improvements in the other), it was so far not directly compared to the use of patient-specific connectivity.

So far, the only study that combined both normative and patient-specific connectivity data in the context of DBS was carried out by Baldermann and colleagues (Baldermann et al., 2019) in 22 patients suffering from Obsessive Compulsive Disorder. Here, patient-specific data in 10 patients were available but lacked in the remaining 12. When optimal connectivity profiles associated with high clinical improvement were estimated based on these 12 patients using a normative connectome, the outcome in the remaining 10 could be predicted by use of their patient-specific connectivity data ($R = 0.7$, $p = 0.01$). The same was true for the opposite case ($R = 0.6$, $p = 0.02$). Indirectly, this finding suggested that normative connectomes could be used to define models of optimal connectivity that would remain predictive when applying patient-specific connectivity datasets.

Here, we directly compared patient-specific connectivity estimates to the ones derived from group connectomes (which were either age-/disease-matched or even acquired in a young-/healthy cohort). We show that optimal connectivity profiles that were associated with good clinical improvement in our sample followed the same overall distribution irrespective of the applied connectivity metric. Namely, functional connectivity with M1 was negatively associated with optimal improve-

ment while more frontal regions (such as SMA, pre-SMA and dorsomedial PFC) were positively associated. Using either method, connectivity profiles were able to account for part of the variance in clinical improvement in out-of-sample patients (leave-one-out design). Moreover, a previously published model of optimal connectivity was associated with clinical outcome using either method. This finding is crucial since it shows that optimal profiles could potentially be estimaged based on large cohorts (and even using normative connectomes) and still applied to patient-specific data. Especially when aggregating large cohorts of DBS patients, it may be complicated if not impossible to obtain diffusion-weighted imaging data from all patients, as well. For instance, large clinical endeavors such as the Early-Stim study cohort (Schuepbach et al., 2013) or the nonmotor study cohort of the International Parkinson and Movement Disorder Society (Dafsari et al., 2018) were acquired without diffusion-weighted imaging data but could still be used to inform optimal symptom-specific connectivity profiles. Similarly, some DBS cohorts are rare or unique world-wide and individualized connectivity data was not acquired for them. Examples include patients suffering from Alzheimer's Disease stimulated with fornical DBS within the AD-vance trials (Laxton et al., 2010), DBS cohorts suffering from rare diseases such as Tourette's Syndrome ()Johnson, et al., 2020 or STN-DBS datasets for treatment of cervical dystonia (Ostrem et al., 2011).

4.2. The case for using brain connectivity to investigate STN-DBS

Several studies have found significant relationships between electrode placements and clinical outcome, without the need to add connectivity information. Specifically, the same optimal target coordinate within the dorsolateral STN was defined by four independent studies, and three of them showed significant correlations between proximity to this coordinate and resulting clinical improvements (Akram et al., 2017; Bot et al., 2018; Horn et al., 2019; Nguyen et al., 2019). If such a clear relationship between the local stimulation sites and clinical improvements exist, why should we investigate connectomic mapping at all? The variance in clinical outcomes explained by such coordinate-based approaches is in the same ballpark of the one explained by brain connectivity in the present study. So, what is the added value?

First, brain connectivity may bear insights into the mechanism of action of DBS. The concept that strong connectivity to M1 is contraproductive for optimal outcomes but more frontal connections seem favorable qualitatively goes beyond knowledge of an optimal sweet-spot in the STN. From such knowledge, we may derive pathophysiological models and translate findings between systems neuroscience and animal models.

Second, brain connectivity could at some point be applied to explore variance in clinical outcome of novel patients, potentially even before surgery. For instance, work by Muthuraman and colleagues showed that atrophy in the SMA before surgery was associated with poor clinical outcome following DBS, matching present connectivity findings (Muthuraman et al., 2017).

Third, individual patient specific connectivity may differ from the norm and could one day help identify patient-specific DBS targets. In Essential Tremor, where clear associations between clinical outcome and a specific structural bundle (the dentatothalamic tract) have been established, this concept has already become clinical practice (Coenen et al., 2014). Similar concepts have been methodically explored using functional MRI (Andersen and Buneo, 2002). So far, to the best of our knowledge, whole-brain connectivity profiles as the ones explored here have not been used in clinical practice, although the general concept has been introduced in 2015 (Fernandes et al., 2015).

Fourth, networks that lead to side-effects when stimulated could be identified. For instance, Irmen and colleagues recently reported a connectivity profile that was associated with depressive symptoms following STN-DBS in PD (Irmen et al., 2019). Crucially, this network, centered on the left dorsolateral prefrontal cortex, could be reproduced in three international cohorts and was successfully used to cross-predict depressive symptom changes across all cohorts. Such a robust map of a circuit that leads to depressive symptoms could be useful to inform stimulation sites that should be avoided. In Essential Tremor, Al-Fatly and colleagues similarly defined networks that were associated with the occurrence of side-effects such as ataxia and dysarthria (Al-Fatly et al., 2019).

Finally, connectivity profiles could be used to bridge fields of invasive and noninvasive brain stimulation. In 2014, Fox and colleagues demonstrated that across 14 diseases, the same networks seem to be modulated by both invasive and noninvasive neuromodulation (Fox et al., 2014). In PD, excitatory TMS to M1 and inhibitory TMS to SMA had beneficial effects (the opposite cases did not). If DBS is seen congruent to a functional lesion (i.e. to disrupt information flow within a specific network), this finding is in agreement with optimal connectivity profiles defined here.

Thus, it seems sensible to investigate brain connectivity measures in the DBS field for reasons that go beyond finding an optimal target coordinate. The question is which connectivity metric should best be used. We discuss the advantages of normative vs. patient-specific connectivity data in the following.

4.3. Pros and Cons of normative vs. patient-specific connectivity data

In a number of studies, network targets were identified by using connectivity data that was *not* derived from each individual patient (Al-Fatly et al., 2019; Baldermann et al., 2019; Calabrese et al., 2015; Cash et al., 2019; Horn et al., 2017b; Petersen et al., 2019; Weigand et al., 2018). One reason for this is data quality. For instance, Calabrese et al. applied a 200 μm isotropic postmortem scan of the brainstem acquired at 7T to be able to resolve the Wernekinck decussation of the dentatothalamic tract. Weigand et al. applied functional imaging data which was averaged across 1000 subjects, leading to a high signal-to-noise ratio (Yeo et al., 2011). The structural connectome used in Horn et al. was acquired on a customized Siemens 3T Connectom scanner with multi-shell diffusion-encoding gradients and b-values reaching up to 10,000 s/mm^2 (Setsompop et al., 2013). Given the strong limitations of diffusion-MRI in general, Petersen and colleagues abandoned MRI-based connectivity altogether and instead created a realistic tract-atlas based on prior anatomical knowledge (Petersen et al., 2019). Hence, normative connectome datasets are of highest quality which may not be straightforward to match during routine preoperative clinical scans in every DBS center. Quality obtained from postmortem connectomes (where scanning times over >24 h are typical) may never be achieved in the living brain of individual patients. Introduction of clinically approved 7T systems may offer novel opportunities for preoperative imaging in the near future.

Along the same lines, investigating each patient's individualized connectivity data is challenging due to poor signal-to-noise and test-retest reliability. This was demonstrated in a study by Petersen and colleagues in which the same subject was scanned ten times. In each, the peak of connectivity to motor-/premotor cortices was identified within the STN (Petersen et al., 2017). Distances across peaks were 0.5–1 mm on average. While this subject was scanned using state-of-the-art methods, test-retest reliability will likely be poorer in clinical datasets acquired in movement disorder patients. A variability of ~1 mm may seem low at first glance but represents half the distance between two DBS contacts and is in the order of distances between responding and non-responding DBS patients (Horn et al., 2019). Moreover, the displacement between some runs was found to be of several millimeters, transposing the peak of M1-connectivity from the sensorimotor to the associative functional zone of the STN. In a similar study with even more pessimistic outcome, Jakab and colleagues repeated scans of the same subjects on different MRI scanners (Jakab et al., 2016). Authors used connectivity data to create thalamic subparcellations relevant for DBS surgery (such as the ventral intermediate nucleus). Variability of these targets introduced by the choice of MRI hardware was similar or higher to inter-subject vari-

ability (!). Moreover, the variability introduced by the MRI hardware made it obvious that single-subject tractography may not be an optimal choice to define surgical targets (see Fig. 6 in the publication by Jakab and colleagues).

Despite the practical and theoretical advantages of normative connectomes and the shortcomings of individual diffusion MRI data, the latter still is needed to reach an ultimate goal of realizing personalized deep brain stimulation. How could the gains of individualized connectivity be combined with the robustness of normative connectomes? One answer would be to scan patients repeatedly and to quantify test-retest reliability. For instance, the midnight scan club endeavor acquired MRI based (but functional) connectivity data of the same subjects in 12 imaging sessions (Gordon et al., 2017). Doing so in each patient that undergoes DBS surgery is impractical and would be very demanding for patients. However, the dataset was recently used to investigate individualized vs. group-level connectivity-based DBS targets (Greene et al., 2019). Similarly, 45 of the 1200 human connectome project participants were scanned twice to allow for quantification of retest error (Van Essen et al., 2013). Such openly available datasets may be used to investigate the test-retest reliability of individualized subjects, while similar data would be needed in patients that will actually undergo DBS afterwards.

An additional strategy could be to *integrate* patient-specific and normative connectomes and yield hybrid estimates. Patient-specific connectivity-profiles could be matched to variants that are robustly found within large normative cohorts and thus used to reshape normative connectomes. This concept could be used to reduce the amount of noise in individualized patient acquisitions, but such an approach would require further methodological work and validation studies.

This being said, we should not ignore the fact that all group studies will require co-registrations from the group connectome to the patient or vice-versa. This process will introduce registration bias. New methods for direct dMRI registrations are being developed and will hopefully become broadly available. Meanwhile, image acquisitions in single patients and MRI technology are also improving. Thus, while group connectomes are currently useful to investigate general relationships between clinical improvement and electrode connectivity, in the future, as the quality and speed of patient specific dMRI sequences improve, the indication or need for group average templates may be challenged.

4.4. Limitations

There are several limitations that apply to the current study. First, heterogeneity, such as the differences in the MRI acquisition protocol and assessments of UPDRS-III between the three cohorts should be considered. Slight differences between raters of symptom scores cannot be ruled out, although the UPDRS-III has a comparably high inter-rater reliability (e.g. intra-class correlation of 0.95 reported in de Deus Fonticoba et al., 2019). Aggregation of datasets was necessary to obtain a large enough sample size and should bias our out-of-sample prediction results toward non-significance. Also, it may match the heterogeneity of clinical DBS cohorts that are usually aggregated across centers in clinical (e.g. Schuepbach et al., 2013). Second, inaccuracies in lead localization result from the approach of mapping electrodes into MNI space. To minimize the amount of error introduced by this step, we applied a modern neuroimaging pipeline that was specifically designed for the task at hand. Processing approaches that were designed to reduce error included brain shift correction, multispectral normalization with subcortical refinement steps (Horn et al., 2019) and a phantom-validated electrode localization approach (Husch et al., 2018). The normalization strategy applied here was recently evaluated by two international teams and led to automatic segmentations of the STN that were nearly as precise as manual expert segmentations (Ewert et al., 2019b; Vogel et al., 2020). Each step of the pipeline was carefully assessed and corrected if needed. Still, the processing steps include errors that could be further reduced by acquiring data of higher resolution as well as test-retest datasets (see above).

Movement artifacts are another limitation that are especially relevant in a cohort suffering from movement disorders. This favors shorter acquisition protocols and the one used in our sample – albeit representative for clinical datasets – may not have been optimal in this regard. Similar dataset quality could potentially have been acquired in less time by applying multiband sequences or similar methods (Harms et al., 2018). We report frame-to-frame movement parameters for the present sample and the average values did not correlate with prediction errors of our model. Still, movement errors do constitute a problem and are likely even more substantial when studying patients suffering from hyperkinetic symptoms such as in tremor dominant PD, Tourette's syndrome or dystonia.

A large limitation that applies to both individualized and normative connectivity mapping can be seen in diffusion MRI in general. Tractography using typical methods on diffusion MRI datasets was recently found to include four times the amount of false-positive tracts as true-positive tracts (Maier-Hein et al., 2017). This fundamental problem has led other groups that investigate similar topics to abandon dMRI based tractography altogether and to instead use detailed literature- and expert-based anatomical knowledge (Gunalan et al., 2017; Petersen et al., 2019). Together with poor test–retest reliability outlined above, these issues challenge the overall concept of connectomic DBS. It remains to be seen whether dMRI based tractography may indeed hold up to some of the promises outlined here, in the future (or not). While our results indicate that significant relationships between connectivity profiles and clinical improvements may be observed, this does not mean that these correlations are significant to clinical practice. Currently, these models are not suitable to predict outcomes in individual patients. Further improvements in diffusion imaging, with higher spatial and angular resolution and improved MRI gradients could add to the value of this modality (Jbabdi and Johansen-Berg, 2011; Sotiropoulos et al., 2013). The choice of whole-brain tractography as well as deterministic tractography on average likely lead to less streamlines to be connected to each VTA (Maier-Hein et al., 2017).

Furthermore, the use of high-resolution postmortem connectome data that is available in submillimeter resolution could be advantageous to employ, as well (Calabrese et al., 2015; again with the same inherent problem of lacking patient-specificity).

Finally, the optimal connectivity model in the current study was based on full UPDRS-III scores which included multiple symptoms in PD patients, such as tremor, bradykinesia, and rigidity. While the current study was not powered to investigate symptom-specific network fingerprints and addressed a different question, future studies could investigate symptom-specific network effects.

5. Conclusions

Our study analyzed optimal connectivity profiles seeding from STN-DBS electrodes based on patient-specific vs. group-level structural connectivity profiles. We demonstrate that on a group level, results from individualized, age- and disease-matched connectomes and healthy-/young connectomes are comparable but not completely interchangeable. Although differences were not significant, results suggest that individualized structural connectivity has the potential to estimate clinical outcomes following STN-DBS slightly better. Still, the use of normative connectomes seems sensible in cases where individualized connectivity data is lacking.

Credit author statement

QW and AH conceptualized the study, wrote the manuscript and acquired funding for the project. QW created figures and conducted analyses. HA, MM, GG-E, SAS, SG, NV-A and LZ collected data, provided critical methodological and conceptual advise and edited the manuscript. SO, NL and AH conducted additional analyses and wrote code used for in analyses. F-CY conducted analyses, created figures and wrote code

used for in analyses. AAK provided resources, critical methodological and conceptual advise and edited the manuscript.

Acknowledgments

This study was supported by the German Research Foundation (DFG grant SPP2041, "Clinical connectomics: a network approach to deep brain stimulation" to AAK as well as Emmy Noether Grant 410169619 to AH). QW was supported by the China Scholarship Council (CSC).

The study was further funded by the Deutsche Forschungsgemeinschaft (DFG, German Research Foundation) – Project-ID 424778381 – TRR 295.

LZ and HA are supported by a grant from the Brain Research Trust (157806) and the National Institute for Health Research University College London Hospitals Biomedical Research Centre. The Unit of Functional Neurosurgery is supported by the Parkinson's Appeal and the Sainsbury Monument Trust. The Wellcome Trust Centre for Neuroimaging is supported by core funding from the Wellcome Trust (091593/Z/10/Z).

SG and MM was supported by the German Research Foundation [grant number: CRC-1193-B05, CRC-TR-128-B05, Abbott ISS study-16429 and Boehringer Ingelheim Funds [grant number: BIF-03].

Data collection and sharing for this project were provided by the Human Connectome Project (HCP; principal investigators: Bruce Rosen, MD, PhD, Arthur W. Toga, PhD, Van J. Weeden, MD). HCP funding was provided by the NIH National Institute of Dental and Craniofacial Research, National Institute of Mental Health, and National Institute of Neurological Disorders and Stroke. HCP data are disseminated by the Laboratory of Neuro Imaging at the University of Southern California. HCP is the result of efforts of coinvestigators from the University of Southern California, Martinos Center for Biomedical Imaging at Massachusetts General Hospital, Washington University, and University of Minnesota.

Data used in the preparation of this article were obtained from the PPMI database (www.ppmi-info.org/ data). For up-to-date information on the study, visit www.ppmi-info.org. PPMI, a public–private partnership, is funded by the Michael J. Fox Foundation for Parkinson's Research. For funding partners, see www.ppmi-info. org/fundingpartners.

Supplementary materials

Supplementary material associated with this article can be found, in the online version, at doi:10.1016/j.neuroimage.2020.117307.

References

Accolla, E.A., Herrojo Ruiz, M., Horn, A., Schneider, G.-H., Schmitz-Hübsch, T., Draganski, B., Kühn, A.A., 2016. Brain networks modulated by subthalamic nucleus deep brain stimulation. Brain 139, 2503–2515. doi:10.1093/brain/aww182.

Akram, H., Georgiev, D., Mahlknecht, P., Hyam, J., Foltynie, T., Limousin, P., Jahanshahi, M., Hariz, M., Zrinzo, L., Ashburner, J., Behrens, T., Sotiropoulos, S.N., Jbabdi, S., De Vita, E., 2017. Subthalamic deep brain stimulation sweet spots and hyperdirect cortical connectivity in Parkinson's disease. NeuroImage 158, 332–345. doi:10.1016/j.neuroimage.2017.07.012.

Al-Fatly, B., Ewert, S., Kübler, D., Kroneberg, D., Horn, A., Kühn, A.A., 2019. Connectivity profile of thalamic deep brain stimulation to effectively treat essential tremor. Brain 142, 3086–3098. doi:10.1093/brain/awz236.

Andersen, R.A., Buneo, C.A., 2002. Intentional maps in posterior parietal cortex. Annu. Rev. Neurosci. 25, 189–220. doi:10.1146/annurev.neuro.25.112701.142922.

Andersson, J.L.R., Skare, S., Ashburner, J., 2003. How to correct susceptibility distortions in spin-echo echo-planar images: application to diffusion tensor imaging. NeuroImage 20, 870–888. doi:10.1016/S1053-8119(03)00336-7.

Andersson, J.L.R., Sotiropoulos, S.N., 2016. An integrated approach to correction for off-resonance effects and subject movement in diffusion MR imaging. NeuroImage 125, 1063–1078. doi:10.1016/j.neuroimage.2015.10.019.

Ashburner, J., Friston, K.J., 2005. Unified segmentation. NeuroImage 26, 839–851. doi:10.1016/j.neuroimage.2005.02.018.

Astrom, M., Diczfalusy, E., Martens, H., Wardell, K., 2015. Relationship between neural activation and electric field distribution during deep brain stimulation. IEEE Trans. Biomed. Eng. 62, 664–672. doi:10.1109/TBME.2014.2363494.

Avants, B.B., Epstein, C.L., Grossman, M., Gee, J.C., 2008. Symmetric diffeomorphic image registration with cross-correlation: Evaluating automated labeling of elderly and neurodegenerative brain. Med. Image Anal. 12, 26–41. doi:10.1016/j.media.2007.06.004.

Baldermann, J., Hahn, L., Dembek, T., Kohl, S., Kuhn, J., Visser-Vandewalle, V., Horn, A., Huys, D., 2019. Weight change after striatal/capsule deep brain stimulation relates to connectivity to the bed nucleus of the stria terminalis and hypothalamus. Brain Sci. 9, 264. doi:10.3390/brainsci9100264.

Baldermann, J.C., Hardenacke, K., Hu, X., Köster, P., Horn, A., Freund, H.J., Zilles, K., Sturm, V., Visser-Vandewalle, V., Jessen, F., Maintz, D., Kuhn, J., 2018. Neuroanatomical characteristics associated with response to deep brain stimulation of the nucleus basalis of Meynert for Alzheimer's Disease. Neuromodulation doi:10.1111/ner.12626.

Baldermann, J.C., Melzer, C., Zapf, A., Kohl, S., Timmermann, L., Tittgemeyer, M., Huys, D., Visser-Vandewalle, V., Kühn, A.A., Horn, A., Kuhn, J., 2019. Connectivity profile predictive of effective deep brain stimulation in obsessive-compulsive disorder. Biol. Psychiatry 85, 735–743. doi:10.1016/j.biopsych.2018.12.019.

Bot, M., Schuurman, P.R., Odekerken, V.J.J., Verhagen, R., Contarino, F.M., De Bie, R.M.A., van den Munckhof, P., 2018. Deep brain stimulation for Parkinson's disease: defining the optimal location within the subthalamic nucleus. J. Neurol. Neurosurg. Psychiatry 89, 493–498. doi:10.1136/jnnp-2017-316907.

Boutet, A., Jain, M., Elias, G.J.B., Gramer, R., Germann, J., Davidson, B., Coblentz, A., Giacobbe, P., Kucharczyk, W., Wennberg, R.A., Ibrahim, G.M., Lozano, A.M., 2019. Network basis of seizures induced by deep brain stimulation: literature review and connectivity analysis. World Neurosurg. 132, 314–320. doi:10.1016/j.wneu.2019.08.094.

Calabrese, E., Hickey, P., Hulette, C., Zhang, J., Parente, B., Lad, S.P., Johnson, G.A., 2015. Postmortem diffusion MRI of the human brainstem and thalamus for deep brain stimulator electrode localization. Hum. Brain Mapp. 36, 3167–3178. doi:10.1002/hbm.22836.

Cash, R.F.H., Zalesky, A., Thomson, R.H., Tian, Y., Cocchi, L., Fitzgerald, P.B., 2019. Subgenual functional connectivity predicts antidepressant treatment response to transcranial magnetic stimulation: independent validation and evaluation of personalization. Biol. Psychiatry 86, e5–e7. doi:10.1016/j.biopsych.2018.12.002.

Coenen, V.A., Allert, N., Paus, S., Kronenbu¨rger, M., Urbach, H., Ma¨dler, B., 2014. Modulation of the cerebello-thalamo-cortical network in thalamic deep brain stimulation for tremor. Neurosurgery 75, 657–670. doi:10.1227/NEU.0000000000000540.

Corp, D.T., Joutsa, J., Darby, R.R., Delnooz, C.C.S., Van De Warrenburg, B.P.C., Cooke, D., Prudente, C.N., Ren, J., Reich, M.M., Batla, A., Bhatia, K.P., Jinnah, H.A., Liu, H., Fox, M.D., 2019. Network localization of cervical dystonia based on causal brain lesions. Brain doi:10.1093/brain/awz112.

Dafsari, H.S., Silverdale, M., Strack, M., Rizos, A., Ashkan, K., Mahlstedt, P., Sachse, L., Steffen, J., Dembek, T.A., Visser-Vandewalle, V., Evans, J., Antonini, A., Martinez-Martin, P., Ray-Chaudhuri, K., Timmermann, L.EUROPAR and the IPMDS Non Motor PD Study Group, 2018. Nonmotor symptoms evolution during 24 months of bilateral subthalamic stimulation in Parkinson's disease. Mov. Disord. 33, 421–430. doi:10.1002/mds.27283.

de Almeida Marcelino, A.L., Horn, A., Krause, P., Kühn, A.A., Neumann, W.-J., 2019. Subthalamic neuromodulation improves short-term motor learning in Parkinson's disease. Brain 142, 2198–2206. doi:10.1093/brain/awz152.

de Deus Fonticoba, T., Santos García, D., Macías Arribí, M., 2019. Inter-rater variability in motor function assessment in Parkinson's disease between experts in movement disorders and nurses specialising in PD management. Neurologia 34, 520–526. doi:10.1016/j.nrl.2017.03.005.

Deuschl, G., Schade-Brittinger, C., Krack, P., Volkmann, J., Schäfer, H., Bötzel, K., Daniels, C., Deutschländer, A., Dillmann, U., Eisner, W., Gruber, D., Hamel, W., Herzog, J., Hilker, R., Klebe, S., Kloß, M., Koy, J., Krause, M., Kupsch, A., Lorenz, D., Lorenzl, S., Mehdorn, H.M., Moringlane, J.R., Oertel, W., Pinsker, M.O., Reichmann, H., Reuß, A., Schneider, G.H., Schnitzler, A., Steude, U., Sturm, V., Timmermann, L., Tronnier, V., Trottenberg, T., Wojtecki, L., Wolf, E., Poewe, W., Voges, J., 2006. A randomized trial of deep-brain stimulation for Parkinson's disease. N. Engl. J. Med. doi:10.1056/NEJMoa060281.

Edlow, B.L., Mareyam, A., Horn, A., Polimeni, J.R., Witzel, T., Tisdall, M.D., Augustinack, J.C., Stockmann, J.P., Diamond, B.R., Stevens, A., Tirrell, L.S., Folkerth, R.D., Wald, L.L., Fischl, B., van der Kouwe, A., 2019. 7 Tesla MRI of the ex vivo human brain at 100 micron resolution. Sci. Data 6, 244. doi:10.1038/s41597-019-0254-8.

Eggers, C., Kahraman, D., Fink, G.R., Schmidt, M., Timmermann, L., 2011. Akinetic-rigid and tremor-dominant Parkinson's disease patients show different patterns of FP-CIT Single photon emission computed tomography. Mov. Disord. 26, 416–423. doi:10.1002/mds.23468.

Elias, G.J.B., Giacobbe, P., Boutet, A., Germann, J., Beyn, M.E., Gramer, R.M., Pancholi, A., Joel, S.E., Lozano, A.M., 2019. Probing the circuitry of panic with deep brain stimulation: Connectomic analysis and review of the literature. Brain Stimul. doi:10.1016/j.brs.2019.09.010.

Ewert, S., Horn, A., Finkel, F., Li, N., Kühn, A.A., Herrington, T.M., 2019a. Optimization and comparative evaluation of nonlinear deformation algorithms for atlas-based segmentation of DBS target nuclei. NeuroImage 184, 586–598. doi:10.1016/j.neuroimage.2018.09.061.

Ewert, S., Horn, A., Finkel, F., Li, N., Kühn, A.A., Herrington, T.M., 2019b. Optimization and comparative evaluation of nonlinear deformation algorithms for atlas-based segmentation of DBS target nuclei. NeuroImage 184, 586–598. doi:10.1016/j.neuroimage.2018.09.061.

Ewert, S., Plettig, P., Li, N., Chakravarty, M.M., Collins, D.L., Herrington, T.M., Kühn, A.A., Horn, A., 2018. Toward defining deep brain stimulation targets in MNI space: A subcortical atlas based on multimodal MRI, histology and structural connectivity. NeuroImage 170, 271–282. doi:10.1016/j.neuroimage.2017.05.015.

Fan, L., Li, H., Zhuo, J., Zhang, Y., Wang, J., Chen, L., Yang, Z., Chu, C., Xie, S., Laird, A.R., Fox, P.T., Eickhoff, S.B., Yu, C., Jiang, T., 2016. The human brainnetome atlas: a

new brain atlas based on connectional architecture. Cereb. Cortex 26, 3508–3526. doi:10.1093/cercor/bhw157.

Fernandes, H.M., Van Hartevelt, T.J., Boccard, S.G.J., Owen, S.L.F., Cabral, J., Deco, G., Green, A.L., Fitzgerald, J.J., Aziz, T.Z., Kringelbach, M.L., 2015. Novel fingerprinting method characterises the necessary and sufficient structural connectivity from deep brain stimulation electrodes for a successful outcome. New J. Phys. 17. doi:10.1088/1367-2630/17/1/015001.

Fonov, V., Evans, A.C., Botteron, K., Almli, C.R., McKinstry, R.C., Collins, D.L., 2011. Unbiased average age-appropriate atlases for pediatric studies. NeuroImage 54, 313–327. doi:10.1016/j.neuroimage.2010.07.033.

Fox, M.D., Buckner, R.L., Liu, H., Mallar Chakravarty, M., Lozano, A.M., Pascual-Leone, A., 2014. Resting-state networks link invasive and noninvasive brain stimulation across diverse psychiatric and neurological diseases. Proc. Natl. Acad. Sci. U.S.A. doi:10.1073/pnas.1405003111.

Gordon, E.M., Laumann, T.O., Gilmore, A.W., Newbold, D.J., Greene, D.J., Berg, J.J., Ortega, M., Hoyt-Drazen, C., Gratton, C., Sun, H., Hampton, J.M., Coalson, R.S., Nguyen, A.L., McDermott, K.B., Shimony, J.S., Snyder, A.Z., Schlaggar, B.L., Petersen, S.E., Nelson, S.M., Dosenbach, N.U.F., 2017. Precision functional mapping of individual human brains. Neuron 95, 791–807. doi:10.1016/j.neuron.2017.07.011, e7https://doi.org/.

Greene, D.J., Marek, S., Gordon, E.M., Siegel, J.S., Gratton, C., Laumann, T.O., Gilmore, A.W., Berg, J.J., Nguyen, A.L., Dierker, D., Van, A.N., Ortega, M., Newbold, D.J., Hampton, J.M., Nielsen, A.N., McDermott, K.B., Roland, J.L., Norris, S.A., Nelson, S.M., Snyder, A.Z., Schlaggar, B.L., Petersen, S.E., Dosenbach, N.U.F., 2019. Integrative and network-specific connectivity of the basal ganglia and thalamus defined in individuals. Neuron doi:10.1016/j.neuron.2019.11.012.

Gunalan, K., Chaturvedi, A., Howell, B., Duchin, Y., Lempka, S.F., Patriat, R., Sapiro, G., Harel, N., McIntyre, C.C., 2017. Creating and parameterizing patient-specific deep brain stimulation pathway-activation models using the hyperdirect pathway as an example. PLoS One 12, e0176132. doi:10.1371/journal.pone.0176132.

Hamani, C., Mayberg, H., Stone, S., Laxton, A., Haber, S., Lozano, A.M., 2011. The subcallosal cingulate gyrus in the context of major depression. Biol. Psychiatry. doi:10.1016/j.biopsych.2010.09.034.

Harms, M.P., Somerville, L.H., Ances, B.M., Andersson, J., Barch, D.M., Bastiani, M., Bookheimer, S.Y., Brown, T.B., Buckner, R.L., Burgess, G.C., Coalson, T.S., Chappell, M.A., Dapretto, M., Douaud, G., Fischl, B., Glasser, M.F., Greve, D.N., Hodge, C., Jamison, K.W., Jbabdi, S., Kandala, S., Li, X., Mair, R.W., Mangia, S., Marcus, D., Mascali, D., Moeller, S., Nichols, T.E., Robinson, E.C., Salat, D.H., Smith, S.M., Sotiropoulos, S.N., Terpstra, M., Thomas, K.M., Tisdall, M.D., Ugurbil, K., van der Kouwe, A., Woods, R.P., Zöllei, L., Van Essen, D.C., Yacoub, E., 2018. Extending the human connectome project across ages: imaging protocols for the lifespan development and aging projects. NeuroImage 183, 972–984. doi:10.1016/j.neuroimage.2018.09.060.

Helmich, R.C., Hallett, M., Deuschl, G., Toni, I., Bloem, B.R., 2012. Cerebral causes and consequences of parkinsonian resting tremor: A tale of two circuits? Brain doi:10.1093/brain/aws023.

Horn, A., 2019. The impact of modern-day neuroimaging on the field of deep brain stimulation. Curr. Opin. Neurol. 32, 511–520. doi:10.1097/wco.0000000000000679.

Horn, A., Blankenburg, F., 2016. Toward a standardized structural-functional group connectome in MNI space. NeuroImage 124, 310–322. doi:10.1016/j.neuroimage.2015.08.048.

Horn, A., Kühn, A.A., 2015. Lead-DBS: a toolbox for deep brain stimulation electrode localizations and visualizations. NeuroImage 107, 127–135. doi:10.1016/j.neuroimage.2014.12.002.

Horn, A., Kühn, A.A., Merkl, A., Shih, L., Alterman, R., Fox, M., 2017a. Probabilistic conversion of neurosurgical DBS electrode coordinates into MNI space. NeuroImage doi:10.1016/j.neuroimage.2017.02.004.

Horn, A., Li, N., Dembek, T.A., Kappel, A., Boulay, C., Ewert, S., Tietze, A., Husch, A., Perera, T., Neumann, W.-J., Reisert, M., Si, H., Oostenveld, R., Rorden, C., Yeh, F.-C., Fang, Q., Herrington, T.M., Vorwerk, J., Kühn, A.A., 2019. Lead-DBS v2: Towards a comprehensive pipeline for deep brain stimulation imaging. NeuroImage 184, 293–316. doi:10.1016/j.neuroimage.2018.08.068.

Horn, A., Ostwald, D., Reisert, M., Blankenburg, F., 2014a. The structural-functional connectome and the default mode network of the human brain. NeuroImage 102 (Pt 1), 142–151. doi:10.1016/j.neuroimage.2013.09.069.

Horn, A., Ostwald, D., Reisert, M., Blankenburg, F., 2014b. The structural–functional connectome and the default mode network of the human brain. NeuroImage 102, 142–151. doi:10.1016/J.NEUROIMAGE.2013.09.069.

Horn, A., Reich, M., Vorwerk, J., Li, N., Wenzel, G., Fang, Q., Schmitz-Hübsch, T., Nickl, R., Kupsch, A., Volkmann, J., Kühn, A.A., Fox, M.D., 2017b. Connectivity Predicts deep brain stimulation outcome in Parkinson disease. Ann. Neurol. 82, 67–78. doi:10.1002/ana.24974.

Husch, A., V Petersen, M., Gemmar, P., Goncalves, J., Hertel, F., 2018. PaCER - A fully automated method for electrode trajectory and contact reconstruction in deep brain stimulation. NeuroImage Clin. 17, 80–89. doi:10.1016/j.nicl.2017.10.004.

Huys, D., Kohl, S., Baldermann, J.C., Timmermann, L., Sturm, V., Visser-Vandewalle, V., Kuhn, J., 2019. Open-label trial of anterior limb of internal capsule-nucleus accumbens deep brain stimulation for obsessive-compulsive disorder: Insights gained. J. Neurol. Neurosurg. Psychiatry.

Irmen, F., Horn, A., Mosley, P., Perry, A., Niklas Petry-Schmelzer, J., Dafsari, H.S., Barbe, M., Visser-Vandewalle, V., Schneider, G.-H., Li, N., Kübler, D., Wenzel, G., Kühn, A., 2019. Left prefrontal connectivity links subthalamic stimulation with depressive symptoms in Parkinson's disease. https://doi.org/ 10.1101/665976

Irmen, F., Horn, A., Mosley, P., Perry, A., Petry-Schmelzer, J.N., Dafsari, H.S., Barbe, M., Visser-Vandewalle, V., Schneider, G., Li, N., Kübler, D., Wenzel, G., Kühn, A.A., 2020. Left prefrontal connectivity links subthalamic stimulation with depressive symptoms. Ann. Neurol. 87, 962–975. doi:10.1002/ana.25734.

Jakab, A., Werner, B., Piccirelli, M., Kovács, K., Martin, E., Thornton, J.S., Yousry, T., Szekely, G., O'Gorman Tuura, R., 2016. Feasibility of diffusion tractography for the reconstruction of intra-thalamic and cerebello-thalamic targets for functional neurosurgery: A multi-vendor pilot study in four subjects. Front. Neuroanat. 10. doi:10.3389/fnana.2016.00076.

Jbabdi, S., Johansen-Berg, H., 2011. Tractography: where do we go from here? Brain Connect. doi:10.1089/brain.2011.0033.

Johnson, K.A, Duffley, G., Anderson, D.N., Ostrem, J.L., Welter, M.-L., Baldermann, J.C., Kuhn, J., Huys, D., Visser-Vandewalle, V., Foltynie, T., Zrinzo, L., Hariz, M., Leentjens, A.F.G., Mogilner, A.Y., Pourfar, M.H., Almeida, L., Gunduz, A., Foote, K.D., Okun, M.S., Butson, C.R., 2020. Structural connectivity predicts clinical outcomes of deep brain stimulation for Tourette syndrome. Brain 143, 2607–2623. doi:10.1093/brain/awaa188.

Kahan, J., Mancini, L., Flandin, G., White, M., Papadaki, A., Thornton, J., Yousry, T., Zrinzo, L., Hariz, M., Limousin, P., Friston, K., Foltynie, T., 2019. Deep brain stimulation has state-dependent effects on motor connectivity in Parkinson's disease. Brain 142, 2417–2431. doi:10.1093/brain/awz164.

Laxton, A.W., Tang-Wai, D.F., McAndrews, M.P., Zumsteg, D., Wennberg, R., Keren, R., Wherrett, J., Naglie, G., Hamani, C., Smith, G.S., Lozano, A.M., 2010. A phase I trial of deep brain stimulation of memory circuits in Alzheimer's disease. Ann. Neurol. 68, 521–534. doi:10.1002/ana.22089.

Li, N., Baldermann, J.C., Kibleur, A., Treu, S., Akram, H., Elias, G.J.B., et al., 2020. A unified connectomic target for deep brain stimulation in obsessive-compulsive disorder. Nat. Commun..

Roxanne Lofredi, Cem Georg Auernig, Friederike Irmen, Johanna Nieweler, Wolf-Julian Neumann, Andreas Horn, Gerd-Helge Schneider, Andrea A. Kühn (2020). Subthalamic stimulation impairs stopping of ongoing movements. Brain (in press)

Lozano, A.M., Lipsman, N., 2013. Probing and regulating dysfunctional circuits using deep brain stimulation. Neuron 77, 406–424. doi:10.1016/j.neuron.2013.01.020.

Maier-Hein, K.H., Neher, P.F., Houde, J.C., Côté, M.A., Garyfallidis, E., Zhong, J., Chamberland, M., Yeh, F.C., Lin, Y.C., Ji, Q., Reddick, W.E., Glass, J.O., Chen, D.Q., Feng, Y., Gao, C., Wu, Y., Ma, J., Renjie, H., Li, Q., Westin, C.F., Deslauriers-Gauthier, S., González, J.O.O., Paquette, M., St-Jean, S., Girard, G., Rheault, F., Sidhu, J., Tax, C.M.W., Guo, F., Mesri, H.Y., Dávid, S., Froeling, M., Heemskerk, A.M., Leemans, A., Boré, A., Pinsard, B., Bedetti, C., Desrosiers, M., Brambati, S., Doyon, J., Sarica, A., Vasta, R., Cerasa, A., Quattrone, A., Yeatman, J., Khan, A.R., Hodges, W., Alexander, S., Romascano, D., Barakovic, M., Auría, A., Esteban, O., Lemkaddem, A., Thiran, J.P., Cetingul, H.E., Odry, B.L., Mailhe, B., Nadar, M.S., Pizzagalli, F., Prasad, G., Villalon-Reina, J.E., Galvis, J., Thompson, P.M., Requejo, F.D.S., Laguna, P.L., Lacerda, L.M., Barrett, R., Dell'Acqua, F., Catani, M., Petit, L., Caruyer, E., Daducci, A., Dyrby, T.B., Holland-Letz, T., Hilgetag, C.C., Stieltjes, B., Descoteaux, M., 2017. The challenge of mapping the human connectome based on diffusion tractography. Nat. Commun. 8. doi:10.1038/s41467-017-01285-x.

Makris, N., Rathi, Y., Mouradian, P., Bonmassar, G., Papadimitriou, G., Ing, W.I., Yeterian, E.H., Kubicki, M., Eskandar, E.N., Wald, L.L., Fan, Q., Nummenmaa, A., Widge, A.S., Dougherty, D.D., 2016. Variability and anatomical specificity of the orbitofrontothalamic fibers of passage in the ventral capsule/ventral striatum (VC/VS): precision care for patient-specific tractography-guided targeting of deep brain stimulation (DBS) in obsessive compulsive disorder (OCD). Brain Imaging Behav. 10, 1054–1067. doi:10.1007/s11682-015-9462-9.

Marek, K., Jennings, D., Lasch, S., Siderowf, A., Tanner, C., Simuni, T., Coffey, C., Kieburtz, K., Flagg, E., Chowdhury, S., Poewe, W., Mollenhauer, B., Sherer, T., Frasier, M., Meunier, C., Rudolph, A., Casaceli, C., Seibyl, J., Mendick, S., Schuff, N., Zhang, Y., Toga, A., Crawford, K., Ansbach, A., de Blasio, P., Piovella, M., Trojanowski, J., Shaw, L., Singleton, A., Hawkins, K., Eberling, J., Russell, D., Leary, L., Factor, S., Sommerfeld, B., Hogarth, P., Pighetti, E., Williams, K., Standaert, D., Guthrie, S., Hauser, R., Delgado, H., Jankovic, J., Hunter, C., Stern, M., Tran, B., Leverenz, J., Baca, M., Frank, S., Thomas, C.A., Richard, I., Deeley, C., Rees, L., Sprenger, F., Lang, E., Shill, H., Obradov, S., Fernandez, H., Winters, A., Berg, D., Gauss, K., Galasko, D., Fontaine, D., Mari, Z., Gerstenhaber, M., Brooks, D., Malloy, S., Barone, P., Longo, K., Comery, T., Ravina, B., Grachev, I., Gallagher, K., Collins, M., Widnell, K.L., Ostrowizki, S., Fontoura, P., La-Roche, F.H., Ho, T., Luthman, J., van der Brug, M., Reith, A.D., Taylor, P., 2011. The Parkinson progression marker initiative (PPMI). Prog. Neurobiol. doi:10.1016/j.pneurobio.2011.09.005.

Mayka, M.A., Corcos, D.M., Leurgans, S.E., Vaillancourt, D.E., 2006. Three-dimensional locations and boundaries of motor and premotor cortices as defined by functional brain imaging: A meta-analysis. NeuroImage 31, 1453–1474. doi:10.1016/j.neuroimage.2006.02.004.

Middlebrooks, E.H., Grewal, S.S., Stead, M., Lundstrom, B.N., Worrell, G.A., Van Gompel, J.J., 2018. Differences in functional connectivity profiles as a predictor of response to anterior thalamic nucleus deep brain stimulation for epilepsy: a hypothesis for the mechanism of action and a potential biomarker for outcomes. Neurosurg. Focus 45, E7. doi:10.3171/2018.5.FOCUS18151.

Muthuraman, M., Deuschl, G., Koirala, N., Riedel, C., Volkmann, J., Groppa, S., 2017. Effects of DBS in parkinsonian patients depend on the structural integrity of frontal cortex. Sci. Rep. 7. doi:10.1038/srep43571.

Muthuraman, M., Raethjen, J., Koirala, N., Anwar, A.R., Mideksa, K.G., Elble, R., Groppa, S., Deuschl, G., 2018. Cerebello-cortical network fingerprints differ between essential, Parkinson's and mimicked tremors. Brain 141, 1770–1781. doi:10.1093/brain/awy098.

Neumann, W.-J., Schroll, H., de Almeida Marcelino, A.L., Horn, A., Ewert, S., Irmen, F., Krause, P., Schneider, G.-H., Hamker, F., Kühn, A.A., 2018. Functional segregation of basal ganglia pathways in Parkinson's disease. Brain 141, 2655–2669. doi:10.1093/brain/awy206.

Nguyen, T.A.K., Nowacki, A., Debove, I., Petermann, K., Tinkhauser, G., Wiest, R., Schüpbach, M., Krack, P., Pollo, C., 2019. Directional stimulation of subthalamic nucleus

sweet spot predicts clinical efficacy: Proof of concept. Brain Stimul. 12, 1127–1134. doi:10.1016/j.brs.2019.05.001.

Ostrem, J.L., Racine, C.A., Glass, G.A., Grace, J.K., Volz, M.M., Heath, S.L., Starr, P.A., 2011. Subthalamic nucleus deep brain stimulation in primary cervical dystonia. Neurology doi:10.1212/WNL.0b013e31820f2e4f.

Pernet, C.R., Wilcox, R., Rousselet, G.A., 2013. Robust correlation analyses: False positive and power validation using a new open source Matlab toolbox. Front. Psychol. 3. doi:10.3389/fpsyg.2012.00606.

Petersen, M.V, Lund, T.E., Sunde, N., Frandsen, J., Rosendal, F., Juul, N., Østergaard, K., 2017. Probabilistic versus deterministic tractography for delineation of the cortico-subthalamic hyperdirect pathway in patients with Parkinson disease selected for deep brain stimulation. J. Neurosurg. 126, 1657–1668. doi:10.3171/2016.4.JNS1624.

Petersen, M.V, Mlakar, J., Haber, S.N., Parent, M., Smith, Y., Strick, P.L., Griswold, M.A., McIntyre, C.C., 2019. Holographic reconstruction of axonal pathways in the human brain. Neuron 104, 1056–1064. doi:10.1016/j.neuron.2019.09.030.

Ponce, F.A., Asaad, W.F., Foote, K.D., Anderson, W.S., Cosgrove, G.R., Baltuch, G.H., Beasley, K., Reymers, D.E., Oh, E.S., Targum, S.D., Smith, G.S., Lyketsos, C.G., Lozano, A.M., 2016. Bilateral deep brain stimulation of the fornix for Alzheimer's disease: Surgical safety in the ADvance trial. J. Neurosurg. doi:10.3171/2015.6.JNS15716.

Schaltenbrand, G, W.W., 1977. Atlas for Stereotaxy of the Human Brain With an Accompanying Guide, 2nd ed. Thieme, Stuttgart LB – SchxTHIEME77.

Schuepbach, W.M.M., Rau, J., Knudsen, K., Volkmann, J., Krack, P., Timmermann, L., Hälbig, T.D., Hesekamp, H., Navarro, S.M., Meier, N., Falk, D., Mehdorn, M., Paschen, S., Maarouf, M., Barbe, M.T., Fink, G.R., Kupsch, A., Gruber, D., Schneider, G.H., Seigneuret, E., Kistner, A., Chaynes, P., Ory-Magne, F., Brefel Courbon, C., Vesper, J., Schnitzler, A., Wojtecki, L., Houeto, J.L., Bataille, B., Maltête, D., Damier, P., Raoul, S., Sixel-Doering, F., Hellwig, D., Gharabaghi, A., Krüger, R., Pinsker, M.O., Amtage, F., Régis, J.M., Witjas, T., Thobois, S., Mertens, P., Kloss, M., Hartmann, A., Oertel, W.H., Post, B., Speelman, H., Agid, Y., Schade-Brittinger, C., Deuschl, G., 2013. Neurostimulation for Parkinson's disease with early motor complications. N. Engl. J. Med. doi:10.1056/NEJMoa1205158.

Setsompop, K., Kimmlingen, R., Eberlein, E., Witzel, T., Cohen-Adad, J., McNab, J.A., Keil, B., Tisdall, M.D., Hoecht, P., Dietz, P., Cauley, S.F., Tountcheva, V., Matschl, V., Lenz, V.H., Heberlein, K., Potthast, A., Thein, H., Van Horn, J., Toga, A., Schmitt, F., Lehne, D., Rosen, B.R., Wedeen, V., Wald, L.L., 2013. Pushing the limits of in vivo diffusion MRI for the Human Connectome Project. NeuroImage doi:10.1016/j.neuroimage.2013.05.078.

Smith, S.M., Jenkinson, M., Woolrich, M.W., Beckmann, C.F., Behrens, T.E.J., Johansen-Berg, H., Bannister, P.R., De Luca, M., Drobnjak, I., Flitney, D.E., Niazy, R.K., Saunders, J., Vickers, J., Zhang, Y., De Stefano, N., Brady, J.M., Matthews, P.M., 2004. Advances in functional and structural MR image analysis and implementation as FSL. NeuroImage doi:10.1016/j.neuroimage.2004.07.051.

Sotiropoulos, S.N., Jbabdi, S., Xu, J., Andersson, J.L., Moeller, S., Auerbach, E.J., Glasser, M.F., Hernandez, M., Sapiro, G., Jenkinson, M., Feinberg, D.A., Yacoub, E., Lenglet, C., Van Essen, D.C., Ugurbil, K., Behrens, T.E.J., Consortium, WU-Minn HCP, 2013. Advances in diffusion MRI acquisition and processing in the Human Connectome Project. NeuroImage 80, 125–143. doi:10.1016/j.neuroimage.2013.05.057.

Talairach, J., Tournoux, P., 1988. Co-Planar Stereotaxis Atlas of the Human Brain: 3-D Proportional System. Thieme Medical Publisher.

Thomas Yeo, B.T., Krienen, F.M., Sepulcre, J., Sabuncu, M.R., Lashkari, D., Hollinshead, M., Roffman, J.L., Smoller, J.W., Zöllei, L., Polimeni, J.R., Fisch, B., Liu, H., Buckner, R.L., 2011. The organization of the human cerebral cortex estimated by intrinsic functional connectivity. J. Neurophysiol. doi:10.1152/jn.00338.2011.

Treu, S., Strange, B., Oxenford, S., Neumann, W.-J., Kühn, A., Li, N., Horn, A., 2020. Deep brain stimulation: imaging on a group level. NeuroImage, 117018 doi:10.1016/j.neuroimage.2020.117018.

Van Essen, D.C., Smith, S.M., Barch, D.M., Behrens, T.E.J., Yacoub, E., Ugurbil, K., 2013. The WU-Minn human connectome project: an overview. NeuroImage 80, 62–79. doi:10.1016/j.neuroimage.2013.05.041.

Vanegas-Arroyave, N., Lauro, P.M., Huang, L., Hallett, M., Horovitz, S.G., Zaghloul, K.A., Lungu, C., 2016. Tractography patterns of subthalamic nucleus deep brain stimulation. Brain 139, 1200–1210. doi:10.1093/brain/aww020.

Vogel, D., Shah, A., Coste, J., Lemaire, J.-J., Wårdell, K., Hemm, S., 2020. Anatomical brain structures normalization for deep brain stimulation in movement disorders. NeuroImage Clin., 102271 doi:10.1016/j.nicl.2020.102271.

Vorwerk, J., Oostenveld, R., Piastra, M.C., Magyari, L., Wolters, C.H., 2018. The FieldTrip-SimBio pipeline for EEG forward solutions. Biomed. Eng. Online 17, 37. doi:10.1186/s12938-018-0463-y.

Weigand, A., Horn, A., Caballero, R., Cooke, D., Stern, A.P., Taylor, S.F., Press, D., Pascual-Leone, A., Fox, M.D., 2018. Prospective validation that subgenual connectivity predicts antidepressant efficacy of transcranial magnetic stimulation sites. Biol. Psychiatry 84, 28–37. doi:10.1016/j.biopsych.2017.10.028.

Yao, C., Horn, A., Li, N., Lu, Y., Fu, Z., Wang, N., Aziz, T.Z., Wang, L., Zhang, S., 2019. Post-operative electrode location and clinical efficacy of subthalamic nucleus deep brain stimulation in Meige syndrome. Park. Relat. Disord. doi:10.1016/j.parkreldis.2018.05.014.

Yeh, F.C., Panesar, S., Fernandes, D., Meola, A., Yoshino, M., Fernandez-Miranda, J.C., Vettel, J.M., Verstynen, T., 2018. Population-averaged atlas of the macroscale human structural connectome and its network topology. NeuroImage doi:10.1016/j.neuroimage.2018.05.027.

Yeh, F.C., Tseng, W.Y.I., 2011. NTU-90: A high angular resolution brain atlas constructed by q-space diffeomorphic reconstruction. NeuroImage doi:10.1016/j.neuroimage.2011.06.021.

Yeh, F.C., Wedeen, V.J., Tseng, W.Y.I., 2010. Generalized q-sampling imaging. IEEE Trans. Med. Imaging 29, 1626–1635. doi:10.1109/TMI.2010.2045126.